Proceedings of the 2007 International Manufacturing Science And Engineering Conference
MSEC2007
October 15-17, 2007, Atlanta, Georgia, USA

MSEC2007-31189

DESIGN ANALYSIS OF A SPHERICAL MAGNETIC BEARING FOR MULTI-DOF ROTATIONAL STAGE APPLICATIONS

Kok-Meng Lee
Professor, Woodruff School of Mechanical Engineering
Georgia Institute of Technology
Atlanta, GA 30332-0405

Hungsun Son
Ph. D. Candidate, Woodruff School of Mechanical Engineering
Georgia Institute of Technology
Atlanta, GA 30332-0405

Jong Kweon Park
Principal Researcher
Korea Institute of Machinery and Materials (KIMM)
Yusong-gu, Daejeon, Korea

ABSTRACT

This paper presents an analytical method to facilitate design of a spherical magnetic bearing (SMB) for a multi-DOF rotational stage. Both passive and active regulations of the SMB are considered. We formulate the SMB dynamic model along with the method of computing the magnetic force and torque required to null any deviation of the rotor, which requires solving the magnetic field. For this, we introduce and validate a general method, referred to here as distributed-multi- pole (DMP) modeling method which requires only a limited set of known (numerical or experimental) field solutions, to derive closed-form solutions for precise calculation of the magnetic field around a permanent magnet (PM). The DMP method has been validated by comparing its modeled potential field and flux density against analytical solutions, as well as the computed force (using DMP modeled field) against published experimental data; both show excellent agreement. Finally, we demonstrate the concept feasibility of the spherical magnetic bearing, and analyze its dynamics and control performance using the DMP modeled field and computed force/torque.

I. INTRODUCTION

Growing demands for miniature devices in modern industries such as micro-machining of biomedical and optical components along with the trend to downscale equipment for manufacturing these products on "desktops" [1], have motivated the development of novel actuators for machine tools. Precision machining of complex-shaped objects often need high-speed dexterous manipulation of the cutter orientation; this calls for more rotational freedoms (in addition to translations) with a minimum number of passive joints that are common sources of wear and tear. Existing multi-DOF rotational stages typically use a combination of single-axis actuators to control orientation. Driven by the stringent accuracy and tolerance requirements, various forms of micro-motion parallel mechanisms [2-4] with three or more single-axis actuators were proposed. Although these multi-DOF mechanisms are structurally more rigid, they are bulky, require more passive joints than the number of DOF of the motion stage, and offer very limited motion range. Unlike many existing orientation stages, ball-joint-like actuators [5-6] (capable of three-DOF orientation in a single joint) offer an attractive alternative to eliminate motion singularities of the multi-DOF rotational stage.

An essential component in the precision multi-DOF rotational stage is a high-performance contact-free bearing. Existing magnetic bearings are typically designed for generating radial and axial forces/moment to support a single-axial rotating shaft [7] [8] or for regulating translational motions [9] with a very small range of shaft inclination. Magnetic bearings have complicated dynamic motion and are often difficult to stabilize due to vibration caused by unbalanced mass, inertia and any other disturbances [10-12].

Design and control of multi-DOF electromagnetic actuators require a good understanding of the magnetic fields, and involve real-time calculation of magnetic forces. Numerical methods (such as FEM) are computationally expensive for design optimization or real-time control. Due to the lack of time-efficient methods for computing magnetic fields and forces, practitioners have resorted to simple empirical lumped-parameter models that often yield only 1st-order accuracy. An alternative method as a tool to characterize magnetic fields has been based on the concept of a magnetic dipole (originally suggested by Fitz Gerlad in 1883). While the dipole model has been widely used to analyze the magnetic field at a sufficiently large distance for applications [13-15] such as electromagnetic wave propagation (antenna dynamics) and geomagnetism (earth polarization), it generally gives a poor approximation when the length scale of the field is very small. For reasons including compact formulation/solutions and intuitive magnetic fields, many researchers (for examples, [16] and [17]) continue to develop dipole models for analyzing actuator designs involving permanent magnets (PM). Nedelcu *et al*. [16] used a magnetic dipole model to describe the field of a PM-based device, where each PM is modeled as a doublet. While the model in [9] provides a concise computational formula for the field and the energy flow, it has difficulties to obtain an accurate magnetic field. De Visschere [17] later pointed out a number of mistakes when comparing the dipole

approximation [16] against an analytical 2D magnetic field solution of a permanent magnet. The existing single dipole model, which bases on the mathematical theory of a doublet, is often studied in the context of physics and valid only for needle-like magnets; thus, it has very limited applications in modern actuator designs.

Historically, ferromagnetic cores were commonly used in electromagnetic actuators. The widely available high-coercive rare-earth permanent magnets at low cost have begun to change that usage, and air-cored electromagnets are now commonly seen in iron-less motors, and have potential for magnetic bearing applications. To further explore the use of high-coercive rare-earth permanent magnets for actuator applications where multi-DOF motion is of particular concerned, there is a need for a more efficient alternative that helps practitioners analyze designs and avoid costly prototyping. Modern design methodologies rely on analytical models and the magnetic field problems associated with multi-DOF PM-based actuators are rather difficult to model. For these reasons, we present here an innovative SMB, and an analytical method to facilitate its design for use in a multi-DOF rotational stage.

The remainder of this paper offers the following:

1. We begin with the design concept of a SMB for a three-DOF spherical-motor-driven rotational stage, which offers a relatively large range of singularity-free motion while allows for contact-free manipulation.
2. We formulate the dynamic model with the magnetic force/torque required to support the spherical rotor, which requires solving the magnetic field of the permanent magnets. Unlike general numerical methods that solve for the complete field, we introduce the DMP method, which requires a limited set of known field solutions, to derive a closed-form solution for precise calculation of the magnetic field around a PM. As will be illustrated, once the DMP model is found the corresponding magnetic field can be computed efficiently and be applied to the control of the SMB. The DMP models have been validated by comparing against analytical solutions and published experimental data.
3. We demonstrate the concept feasibility of the SMB by analyzing its dynamics using the DMP modeled field and computed force and torque; both passive and active SMB regulations have been considered.

II. DESIGN CONCEPT OF A SMB

Figure 1 illustrates the design concept of a spherical magnetic bearing (SMB), which consists of two functional subsystems; a PM-based bearing system, and an electromagnetic (EM) regulator.

The PM-based SMB (designed to balance the moving stage statically in the absence of any external load) is made up two components; a moving PM embedded in the nonmagnetic spherical rotor on which the shaft for the maching table (not shown) is attached, and two rings of eight PM's. In Fig. 1, the **bold** arrows denote the direction of the PM magnetization.

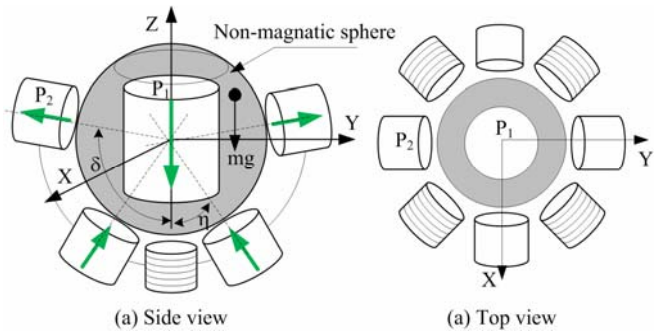

Fig. 1 Design concept of a SMB

The focus here is the design of the SMB for a spherical-motor-driven rotational stage that offers three-DOF ball-joint-like orientation in a single joint. In Fig. 1, the function of the four PM's in the upper ring is primarily to compensate for any gravitational effects on inclination. The four PM's on the lower ring balance the static weight replacing the use of mechanical stabilizing counterweights which would lower the response speed. As shown in Fig. 1, the rotor center is regulated using repulsive magnets. Unlike an attractive pair of magnets which behave as a "mechanical spring with a negative stiffness" and is inherently an unstable system, the combination of an electromagnet (EM) and the two rings of repulsive magnets (which behave essentially as non-contact mechanical springs) tends to drive the rotor center to equilibrium.

The SMB is contact-free and has no mechanical damping; any perturbation on the rotor will result in un-damped oscillations. To decouple the bearing regulation from the orientation control of the spherical motor, five electromagnets are designed to provide electronic damping and active compensation against un-modeled dynamics.

II.1Dynamic Model

The rotor has six-DOF, $\mathbf{q} = \left[\mathbf{q_T}(x, y, z) \quad \mathbf{q_R}(\alpha, \beta, \gamma)\right]^{\mathrm{T}}$ as defined in Fig.2, where h is the deviation of the rotor center with respect to the stator XYZ reference frame.

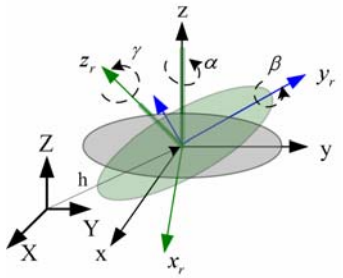

Fig. 2 Coordinate system

In general, the rotor dynamics can be characterized by (1):

$$\mathbf{M}\ddot{\mathbf{q}} + \mathbf{C}(\mathbf{q}, \dot{\mathbf{q}}) + \mathbf{Q} = 0 \qquad (1)$$

where $\mathbf{M}=\begin{bmatrix} m\mathbf{I} & 0 \\ 0 & \mathbf{M_R} \end{bmatrix}$; $\mathbf{C}(\mathbf{q},\dot{\mathbf{q}})=\begin{bmatrix} 0 \\ \mathbf{C_R}(\mathbf{q_R},\dot{\mathbf{q}}_\mathbf{R}) \end{bmatrix}$; $\mathbf{Q}=\begin{bmatrix} \mathbf{Q_T} \\ \mathbf{Q_R} \end{bmatrix}$; m is the mass of the rotor; $\mathbf{M_R}$ is the 3×3 inertia matrix of the rotor; $\mathbf{C_R}(\mathbf{q_R},\dot{\mathbf{q}}_\mathbf{R})$ is an 3×1 vector of centrifugal and Coriolis terms; and $\mathbf{Q_T}$ and $\mathbf{Q_R}$ are the respective generalized force and torque (3×1) vectors which include the gravity terms. For completeness and clarity, the terms in the dynamic equation (1) are detailed in Appendix A, where the center of mass of the moving stage is defined at (x_c, y_c, z_c).

II. 2 Magnetic Forces and Torques

In (1) where the details are given in Appendix A, the forces $\mathbf{F}(F_x, F_y, F_z)$ and torques $\mathbf{T}(T_x, T_y, T_z)$ acting on the boundary of the moving (cylindrical) magnet due to the magnetic field $\mathbf{B}$ can be calculated using Maxwell stress tensor $\mathbf{\Gamma}$ defined as

$$\mathbf{\Gamma}=\frac{1}{\mu_0}\left(\mathbf{B}(\mathbf{B}\bullet\mathbf{n})-\frac{1}{2}|\mathbf{B}|^2\,\mathbf{n}\right) \tag{2}$$

where μ_0 is free space permeability; and $\mathbf{n}$ is the normal of the material interface. For a cylindrical magnet,

$$\mathbf{F}=\sum_{i=1}^{3}\int_{S_i}\mathbf{\Gamma}\bullet\mathbf{n}_i\,dS_i \quad\text{and}\quad \mathbf{T}=\sum_{i=1}^{3}\int_{S_i}\mathbf{r}\times(\mathbf{\Gamma}\bullet\mathbf{n}_i)\,dS_i \tag{3a,b}$$

where $\mathbf{n}_1=-\mathbf{n}_3=[0\ \ 0\ \ 1]^{\mathrm{T}}$ is the surface normal of the top and bottom circular surfaces (S_1 and S_3) respectively; and $\mathbf{n}_2=[\cos\theta\ \ \sin\theta\ \ 0]^{\mathrm{T}}$ is that of the circumferential surface S_2. Since (3) computes the force and torque on the given field, $\mathbf{B}$ is the total magnetic field from both the PM's and EM's modeled in the surface integration.

II.3 Magnetic Field Model

The solutions to the force/torque equations (3a) and (3b) require solving the magnetic field. We model the PM and EM using the concept of distributed multiple poles (DMP). This DMP method provides us a means to derive closed-form solutions for characterizing the magnetic field $\mathbf{B}$ that satisfies the following assumptions: the field is continuous and irrotational; and the medium is homogeneous. These enable us to define a scalar magnetic potential Φ such that the magnetic field intensity $\mathbf{H}$ given by

$$\mathbf{H}=-\nabla\Phi \quad\text{and}\quad \mathbf{B}=\mu_0\mathbf{H} \tag{4}$$

satisfies $\nabla^2\Phi=0$. The solution to Laplace's equation, which satisfies the field for a magnetic pole, is given by

$$\Phi=\frac{(-1)^j}{4\pi R}m \tag{5}$$

where m is the strength of the pole; j takes the value 0 or 1 designating that the pole is a source or a sink respectively; and R is the distance from the pole to the field point. A single pole does not exist alone in a magnet filed; we define a *dipole* here as a pair of source and sink separated by a distance $\bar{\ell}$.

To account for the shape of a physical magnet, we model the cylindrical magnet (radius a, length ℓ and $\mathbf{M}=M_o\mathbf{e}_z$) using multiple dipoles as shown in Fig. 3, where k circular loops (each with radius $\bar{a}_j$) of n dipoles are uniformly spaced in parallel to the magnetization vector.

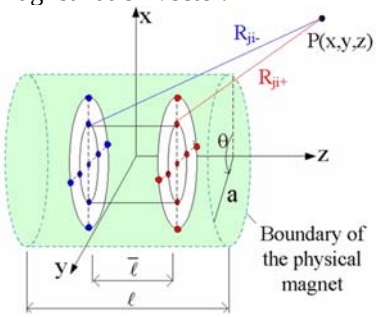

Fig. 3 DMP model of a cylindrical magnet

In Fig. 3, R_{ji+} and R_{ji-}, which are the distances from the i^{th} pair of source and sink respectively in the j^{th} loop to any point $P(x,y,z)$, are given by

$$R_{ji\pm}^2=\left[x-\bar{a}_j\cos i\theta\right]^2+\left[y-\bar{a}_j\sin i\theta\right]^2+\left(z\mp\bar{\ell}/2\right)^2 \tag{6}$$

where $j=0,1,...,k$; $\bar{a}_j=aj/(k+1)$; and $0<\bar{\ell}<\ell$. A general method to determine the unknowns (k, n, $\bar{\ell}$, and m_j where j = 0, …, k) in the DMP model is given in Appendix B. Since Laplace equation is linear, the magnetic field $\Phi(x,y,z)$ of the PM can be obtained by summing the magnetic fields contributed by the individual poles:

$$\Phi=\frac{1}{4\pi}\sum_{j=0}^{k}m_j\sum_{i=1}^{n_k}\left(\frac{1}{R_{ji+}}-\frac{1}{R_{ji-}}\right)$$
$$\text{where}\quad n_k=\begin{cases}1 & \text{if } j=0\\ n & \text{if } j\neq 0\end{cases} \tag{7}$$

Similarly, the magnetic flux density at P can be found from (4). Since $\nabla(1/R)=-\mathbf{a}_R(1/R^2)$ where $\mathbf{a}_R\left(=\mathbf{R}/R\right)$,

$$\mathbf{B}=\frac{\mu_o}{4\pi}\sum_{j=0}^{k}m_j\sum_{i=1}^{n_k}\left(\frac{\mathbf{a}_{Rji+}}{R_{ji+}^2}-\frac{\mathbf{a}_{Rji-}}{R_{ji-}^2}\right) \tag{8}$$

Equations (7) and (8) offer a closed-form solution to determine the 3D magnetic field of a PM. The total field $\mathbf{B}$ can be obtained from the vector sum of the individual fields. The force and torque on the boundary of the moving magnet can be calculated from (3a) and (3b) respectively.

II. 4 Perturbation Dynamics and Feedback Control

To analyze the effect of small perturbations on the dynamics of the multi-DOF orientation stage, we neglect the effect of centrifugal/Coriolis terms, and linearize the rotor dynamics about the desired operating point or $\mathbf{q}_\mathrm{d}=\mathbf{0}$:

$$\hat{\mathbf{M}}\ddot{\mathbf{q}}+\hat{\mathbf{Q}}=\hat{\mathbf{F}}_\mathrm{c} \tag{9}$$

where $\hat{\mathbf{Q}}=\mathbf{Q}-\bar{\mathbf{Q}}$, and $\hat{\mathbf{q}}=\mathbf{q}-\mathbf{q}_\mathrm{d}=\mathbf{q}$. Since the moving magnet is symmetric about the z-axis of the rotor, the spin

angle γ has no effect on the bearing design. Thus, the system requires only five EM's (or voice coils) to control the three translational and two orientation deviations. Based on this, a PD controller (through the five voice coils) can be designed as

$$\hat{\mathbf{F}}_c = -\mathbf{K}_p\mathbf{q} - \mathbf{K}_d\dot{\mathbf{q}} \qquad (10)$$

where $\mathbf{K}_p$ and $\mathbf{K}_d$ are the positive position and velocity control gain matrices.

III. VALIDATION OF DMP MODEL

To validate the DMP model for computing of the magnetic forces and torques, the following two examples are computed.

Example 1: Magnetic field

We model the magnet P_1 ($2a/\ell = 0.75$) and P_2 ($2a/\ell = 1$) as shown in Fig. 1 using the procedure outlined in Appendix B. The values of the PM parameters (both with constant $\mathbf{M} = M_o\mathbf{e}_z$) are tabulated in Table 1.

Table 1 Values of the parameters (k=1, n=6)

Poles Fig. 1(a)	$2a\times\ell$ mm	$\mathbf{M}_o$ Tesla	$\bar{\ell}/\ell$	$\boldsymbol{m}$ (n=1, k=6) $(T/m^2)\times 1.0e\text{-}4$
P_1 (δ=100°)	19.05×25	1.2	0.712	m_o=–0.072; m_{1i}=0.874
P_2 (η=30°)	12.7×12.7	1.2	0.514	m_o=–0.209; m_{1i}=0.567

Rotor radius =19.05mm; gap h = 1 mm; moving mass =5.5 kg

We compute the magnetic potential and flux density along the z-axis and the y direction on $z = \ell/2$ surface. For the purpose of validation, we compare the computed results of the DMP models (7) and (8) against analytical solutions in Fig. 4.

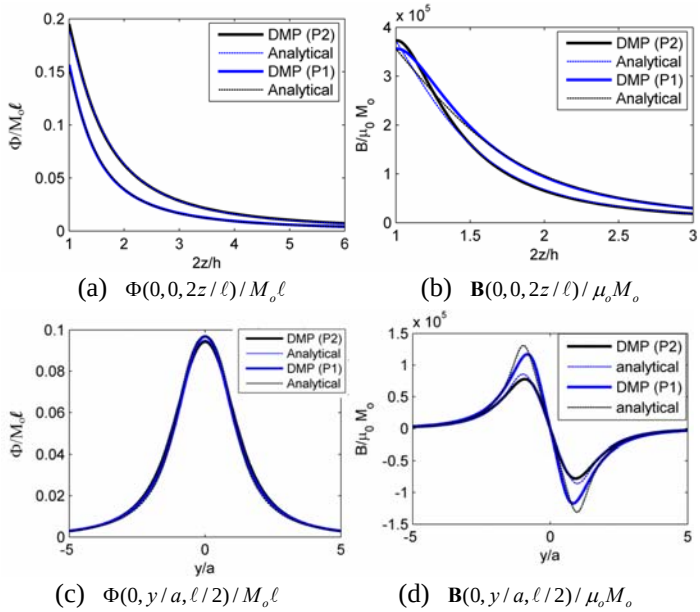

(a) $\Phi(0,0,2z/\ell)/M_o\ell$ (b) $\mathbf{B}(0,0,2z/\ell)/\mu_o M_o$

(c) $\Phi(0,y/a,\ell/2)/M_o\ell$ (d) $\mathbf{B}(0,y/a,\ell/2)/\mu_o M_o$

Fig, 4 Normalized potential and flux density

Since the analytical solutions of the closed-form potential and flux density are available only along the z-axis, which are given respectively by (B.2) and (B.3) in Appendix B, we numerically integrate the general integral given in [18] to obtain the analytical solution of the magnetic scalar potential along the y-axis. To avoid the singularity at the surface, the $\Phi_A(0, y, \ell/2)$ values are solved numerically with $|\mathbf{R}'| + 10^{-6}$; no significant difference in results was found when $\varepsilon_R \le 10^{-3}$. Once Φ_A is found, the magnetic flux density can be computed from (4).

The results are compared in Fig. 4 and Table 2 where the integrated squared-error in Φ is defined in (B.1) and similarly for **B**; the comparison shows excellent agreement. As expected, $\mathbf{B}(0, y/a, 2z/\ell = 1)$ has a higher % error than $\mathbf{B}(0,0,2z/\ell)$ because the computation was near the singularity at the surface.

Table 2: Integrated squared-error (%)

PM	$\Phi(0,0,2z/\ell)/M_o\ell$	$\mathbf{B}(0,0,2z/\ell)/\mu_o M_o$	$\mathbf{B}(0,y/a,\ell/2)/\mu_o M_o$
P_1	1.0827	3.80%	9.84%
P_2	0.9995	3.42%	6.41%

Example 2: Force Computation with DMP Models

To examine the effect of the DMP model on the force computation, we compute the repulsive force between two identical magnets using the Maxwell stress tensor (2) where **B** is the combined field of the two permanent magnets modeled using the DMP method. To validate the DMP-based force computation, this case study modeled the setup given in [19], where the pair of permanent magnets is separately mounted on two cantilever beams. One of magnets is driven by a precision NSK ball-screw while the other carries a strain-gage that measures the repulsion force for a specified distance d between the two PM axes as shown in Fig. 5.

Along with the values characterizing the two identical magnets, the forces computed using the DMP model are compared in Fig. 5 against the three different types of published data given in [19]; namely, the experimentally measured forces, the forces computed using the analytical solutions with Φ integrated numerically, and the forces computed using mesh-less method (MLM) with strong form formulation (SFF).

The comparisons are remarkably close; this validates the DMP modeling method as well as the effectiveness of the closed-form field solutions.

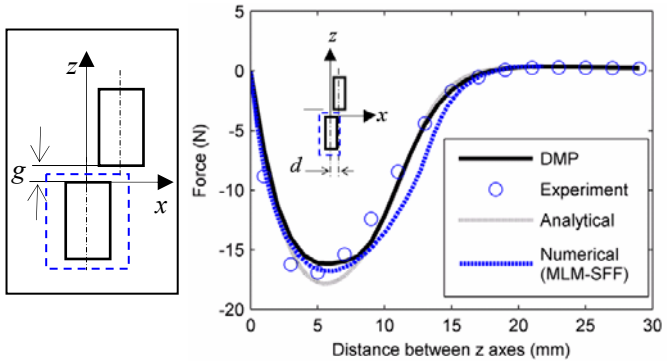

Fig. 5 Repulsion between two PM's [19]

(a= ℓ =6.35mm, air gap g =0.5mm, and $\mu_0 M_0$=1.35T)

IV. SIMULATION RESULTS AND DISCUSSIONS

To illustrate the use of the DMP model for design analysis of the SMB, we compute the magnetic field, forces and torque along the two planes (α=0° and α=45°) as shown in Fig. 6(a) and simulate the perturbation dynamics with and without feedback control.

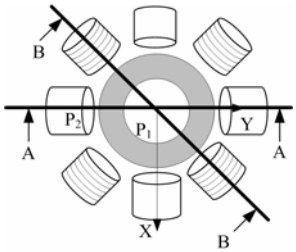

(a) Plan view and view definitions

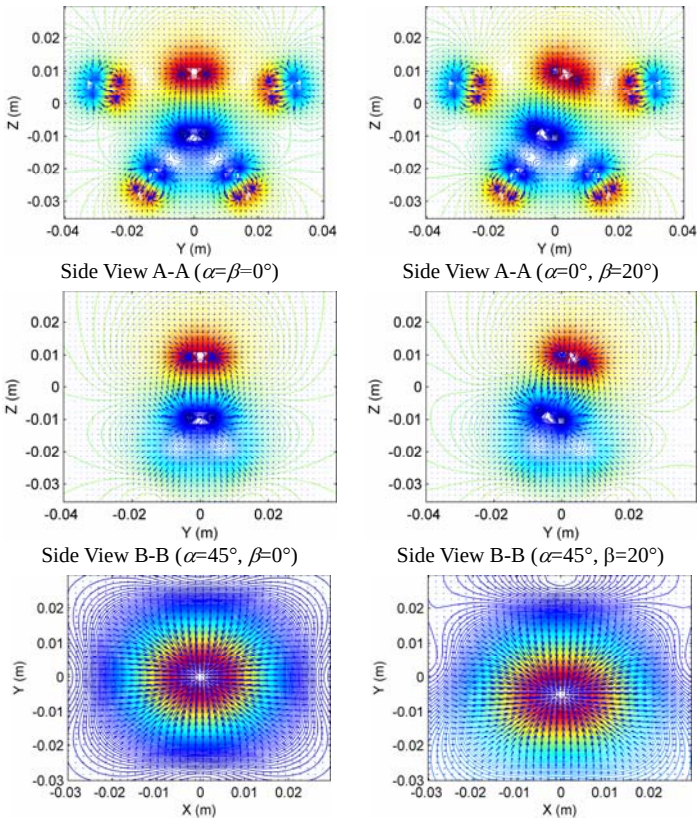

Side View A-A (α=β=0°) Side View A-A (α=0°, β=20°)

Side View B-B (α=45°, β=0°) Side View B-B (α=45°, β=20°)

Plan view (α=β=0°) Plan view (α=0°, β=20°)

(b) no inclination (c) 20° inclination

Fig. 6 Potential and flux density fields

IV.1 Computed Magnetic Fields and Forces of PM's

Figure 6 offers three different views for visualizing the total magnetic field; side view-A-A, side view B-B and plan view as illustrated in Fig. 6(a). Figures 6(b) and (c) graph the magnetic flux lines of the permanent magnets for β=0° and β=20° respectively; as expected, the scalar potential and magnetic flux field are orthogonal to each other.

Once the total magnetic field **B** is known the repulsive forces and torques acting on the moving magnet P_1 can be calculated using (3a,) and (3b) respectively with Maxwell tensor defined in (2). As an illustration, we compute the magnetic forces (F_x and F_z) and torque T_y in the rotor *x-z* plane about the equilibrium point **q**=0. The results are shown in two columns in Fig. 7.

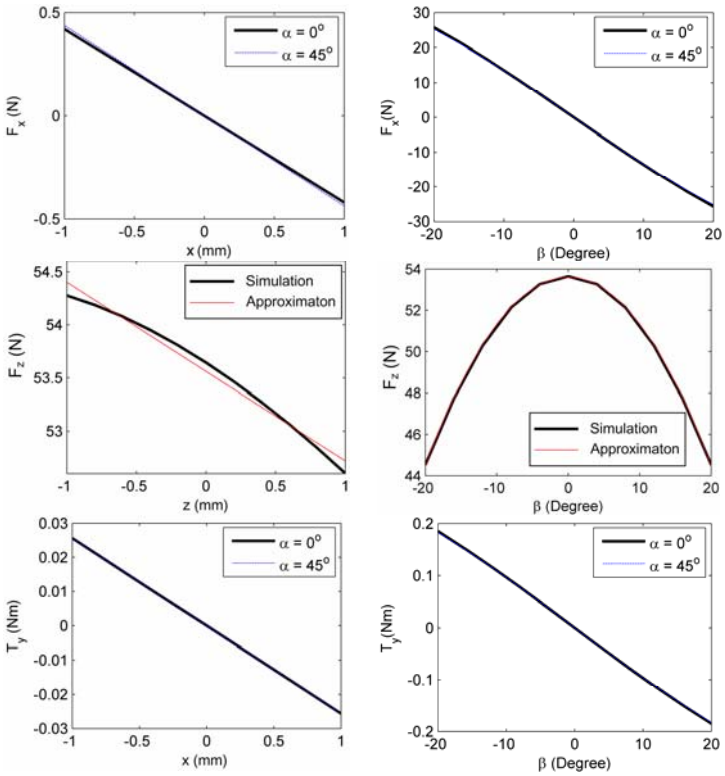

(a) no inclination, β=0 (b) no deviation, x=z=0

Fig. 7 Computed magnetic forces and torques

In Fig. 7(a), the forces and torque are computed as a function of deviations in x or z direction with β=0°. Fig. 7(b) computes the effect of β on the forces and torque. Some observations can be made from the results:

1. The z-component force F_z is dominant, and increases as the z-component deviation decreases; this is expected since the SMB is designed to support the static weight of the moving stage. As shown in Fig. 7(b), F_z has a maximum at β=0° and monotonically reduced by 20% at β=±20°.
2. Although only two orthogonal pairs of stator PM's in an XY plane are used, the magnetic force F_x and torque T_y are relatively uniform within the range of translational motion as shown in Figs. 7(a) and 7(b).

IV. 2 Effect of PD feedback Control on SMB

Because of symmetry, the effect of small displacement variations on the SMB dynamics can be illustrated using the perturbation model in the XZ plane (with $\alpha=\gamma=0$). For a linearized model with $\hat{\mathbf{q}} = \mathbf{q} = [x, z, \beta]^{\mathrm{T}}$, we have in (10),

$$\hat{\mathbf{Q}} = \begin{bmatrix} \hat{F}_x & \hat{F}_z & \hat{T}_y \end{bmatrix}^{\mathrm{T}} \tag{11}$$

and $$\mathbf{M} = dia\left(m, m, (mx_c^2 + z_c^2)\right) \tag{12}$$

where $$\hat{F}_x \approx k_x x + k_1 \beta \tag{13a}$$

$$\hat{F}_z \approx k_z z + k_2 \beta \tag{13b}$$

and $$\hat{T}_y \approx k_R x + k_3 \beta \,. \tag{13c}$$

Along with a listing of the linearized spring constants used in the simulation, Figure 8 shows the responses of the open-loop system to an initial perturbation. Since the system has no mechanical damping, the natural frequencies (eigenvalues) are directly a direct reflection of the equivalent spring constants which are coupled among the *x, z,* and β equations of motion. Thus, the dynamic responses to initial perturbations show a combination of high and low frequencies.

m=5.5kg, x_c=3, z_c=5 mm

$\hat{F}_x \approx k_x x + k_1 \beta$

$k_x = 426.7$N/m

$k_1 = 75.3$Nm/rad

$\hat{F}_z \approx k_z z + k_2 \beta$

$k_z = 841.2$N/m

$k_2 = 148.6$N/rad

$\hat{T}_y \approx k_R x + k_3 \beta$

$k_R = 25.6$Nm/m

$k_3 = 0.54$Nm/rad

Open-loop poles:
±j20.6, ±j2.1,
±j29.0

Initial conditions:
(1mm, 1mm, .01rad)

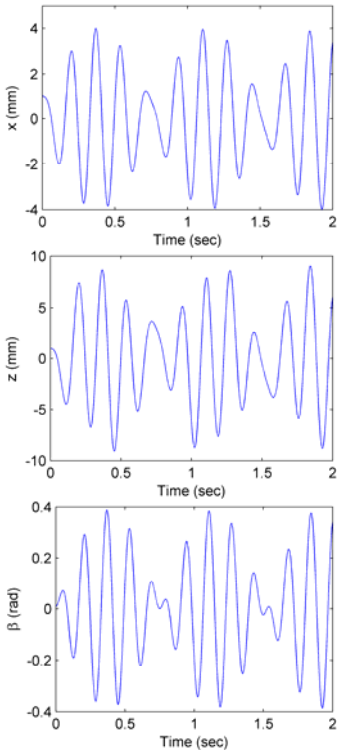

Fig. 8 Open-loop response to initial perturbation

As a comparison, we simulate the closed-loop responses to the same initial perturbation in Fig. 9. The gain matrices of the closed loop system are

$$\mathbf{K}_p = 500\mathbf{I} \quad \text{and} \quad \mathbf{K}_d = 100\mathbf{I} \,.$$

The corresponding closed-loop poles are

–3.84, –2.09, -46.16, –47.91, -5.71, -44.29

The results are given in two column of Fig. 9. As shown in the right column or Fig. 9(a), the responses to the initial perturbation are well damped and require less than 0.5N restoring forces. Clearly, the intent here is to demonstrate the concept feasibility of the SMB. Once the operational principle and the design method of the SBM are proven and well understood, the DMP model can be used to optimize the parameters and to design Hall-effect sensors for the orientation measurements given a magnetic field. The simulation results can be used to design the regulating EM voice coils.

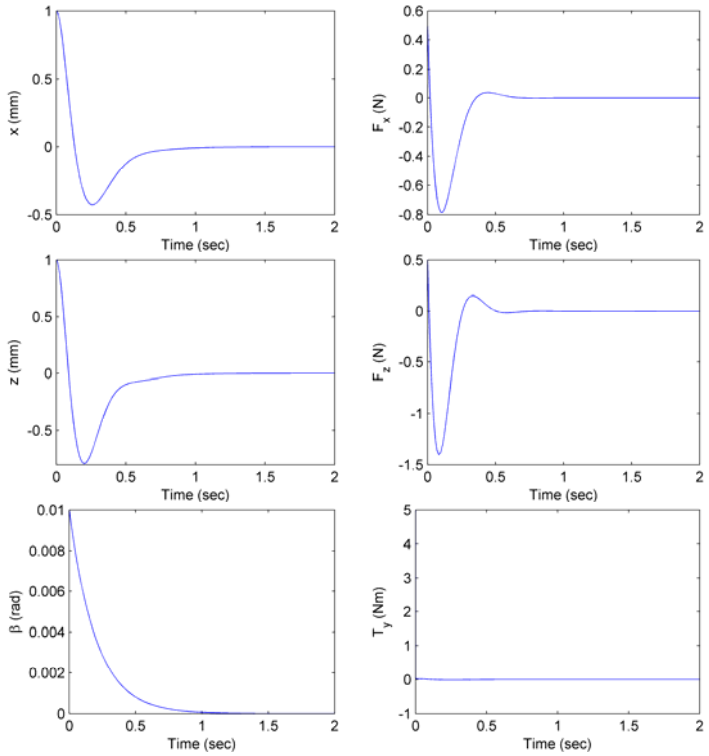

(a) Position and orientation (b) Forces and moment

Fig. 9 Closed-loop response to initial perturbation

V. CONCLUSIONS

We have presented the design concept, dynamic model, and control of a spherical magnetic bearing (SMB), along with the method to compute the magnetic force and torque. We have also introduced the DMP modeling method and derived closed form solutions to characterize the magnetic fields, from which the magnetic force and torque are derived using the Maxwell stress tensor. We also validated the DMP models by comparing the modeled potential field and flux density against analytical solutions, and by comparing the computed forces against published experimental data. Both show excellent agreement. With the validated models, we have demonstrated the concept feasibility of the spherical magnetic bearing by analyzing its dynamics and its control performance.

NOMENCLATURE

Capitalized symbols		Lowercase symbols	
B	Magnetic flux density	*a*	Radius of PM
C	Coriolis matrix	$\boldsymbol{\ell}$	Length of PM
F	*x,y,z* component forces	***m***	Dipole strength
F	Force generated by EM	m	Mass of the stage
T	*x,y,z* component torque	**n**	Surface normal vector
H	Magnetic flux intensity	***k***	Linearized spring constant
I	Moments of inertia	$\mathbf{q_R}$	Rotation vector
M	Mass matrix	**Greek letter symbols**	
$\mathbf{M}_o$	Magnetization vector	α, β, γ	ZYZ Euler angles
S_x	sin (x)	ε_R	Error tolerance
C_x	cos(x)	η, δ	Locations of PM
P_1	Moving PM	μ_o	free space permeability
P_2	Stator PM	Φ	Magnetic potential
Q	Generalized forces/torques	Γ	Maxwell stress tensor matrix

REFERENCES

[1] Park, J. K. “Development of next generation microfactory systems”, 2nd International workshop on Microfactory Technology, 2006 July 6-7.

[2] Lee, K-M. and S. Arjunan, "A three-DOF micro-motion in-parallel actuated manipulator," IEEE Trans. on Robotics and Automation, October 1991, vol. 7, no. 5, pp. 634-641.

[3] Shchokin, B., and F. J.-S., “Design and kinematic analysis of a rotary positioner”, Robotica, v 25 Jan., 2005, pp 75-85.

[4] Ng, C. C., S. K. Ong, and A.Y. C. Nee “Design and development of 3–DOF modular micro parallel kinematic manipulator”, International J. of Advanced Manufacturing Tech., v 31 Mar., 2006.

[5] Lee, K.-M., and C. Kwan, "Design concept development of a spherical stepper for robotic applications*",* IEEE Trans. on Robotics and Automation, 1991. **7**(1), pp. 175-181.

[6] Lee, K.-M. R. A. Sosseh & Z. Wei, “Effects of the Torque Model on the Control of a VR Spherical Motor,” IFAC J. of Contr. Eng. Practice*,* Vol 12/11, 2004, pp 1437-1449.

[7] Meeks, C. R., “Magnetic bearing structure providing radial, axial and moment load bearing support for a rotatable shaft”, U.S Patent 5111102, 1992

[8] Park, J. W., S. K Ro, J. H. Kyung, “Spindle with cone type magnetic bearing”, Korea Patent 1020030069338, 2003.

[9] Hockney, R. L., J. R. Downer, D. B. Eisenhaure, T. J. Hawkey, and B. G. Johnson, “Magnetic translator bearings”**,** U.S Patent 4900962, 1990.

[10] Ryan, S. T., “Dynamically stable magnetic suspension bearing system”, U.S Patent 5495221, 1996.

[11] Herzog, R., P. Buhler, C. Gahler and R. Larsonneur “Unbalance compensation using generalized notch filters in the multivariable feedback of magnetic bearings”, IEEE Trans. on Control Systems Tech., vol. 4., 1996, pp. 1063-6536

[12] Park, J. W., S. K Ro, J. H. Kyung, “Method for controlling position error of a spindle with cone type magnetic bearing.”, Korea Patent 1020040093200, 2004

[13] Craik, D. J., "Magnetostatics of axially symmetric structure”, J. of Physics, 1974. 7 p. 1566.

[14] Green, M. A., "Modeling the behavior of oriented permanent magnet material using current doublet theory”, IEEE Trans. on Magnetics, 1988. March, p. 1528.

[15] Bennett, W. S., "Basic sources of electric and magnetic fields newly examined”, IEEE Antennas and Propagation Magazine, 2001. p. 31-5.

[16] Nedelcu, S. and J. H. P. Watson, "Mangetic dipole model of a permanent magnet based device”, J. of Physics, 2001. p. 2622-2628.

[17] De Visschere P. , "An exact two-dimensional model for a periodic circular array of head-to-head permanent magnets”, J. of Physics D: Applied Physics, 2005, p. 355-362.

[18] Jackson, J.D. "Classical electrodynamics " New York : Wiley, 1999

[19] Lee, K.-M., Qiang Li and H. Son, "Effects of numerical formulation on magnetic field computation using meshless methods," IEEE Trans. on Magnetics, Vol. 42, No. 9, 2006, pp. 2164-2171.

APPENDIX A

EQUATIONS OF THE ROTOR DYNAMICS

The terms in the dynamic equation (1) are given by

$$\mathbf{M_R}=\begin{bmatrix}\left(I_1C_\gamma^2+I_2S_\gamma^2\right)S_\beta^2+I_3S_\beta^2 & \left(I_2-I_1\right)S_\beta S_\gamma C_\gamma & I_3C_\beta\\ \left(I_2-I_1\right)S_\beta S_\gamma C_\gamma & I_2C_\gamma^2+I_1S_\gamma^2 & 0\\ I_3C_\beta & 0 & I_3\end{bmatrix} \tag{A.1}$$

$$\mathbf{C_R}(\mathbf{q_R},\dot{\mathbf{q}}_\mathbf{R})=\begin{bmatrix}C_1 & C_2 & C_3\end{bmatrix}^{\mathrm{T}} \tag{A.2}$$

where

$$\begin{aligned}C_1 &= I_1(\dot\alpha S_\beta C_\gamma-\dot\beta S_\gamma)(\dot\beta C_\beta C_\gamma-\dot\gamma S_\beta S_\gamma)+I_1S_\beta C_\gamma\left[\dot\alpha\dot\beta C_\beta C_\gamma-\dot\gamma(\dot\alpha S_\beta S_\gamma+\dot\beta C_\gamma)\right]\\ &+I_2\dot\gamma S_\beta C_\gamma(\dot\beta C_\gamma+\dot\alpha S_\beta S_\gamma)+I_2S_\beta S_\gamma\left[\dot\alpha\dot\beta C_\beta S_\gamma+\dot\gamma(\dot\alpha S_\beta C_\gamma-\dot\beta S_\gamma)\right]\\ &-I_3\dot\beta S_\beta(\dot\gamma+\dot\alpha C_\beta+\dot\alpha C_\beta)\\ C_2 &= I_1\dot\gamma C_\gamma(\dot\beta S_\gamma-\dot\alpha S_\beta C_\gamma)-I_1S_\gamma\left[\dot\alpha\dot\beta C_\beta C_\gamma-\dot\gamma(\dot\alpha S_\beta S_\gamma+\dot\beta C_\gamma)\right]\\ &-I_2\dot\gamma S_\gamma(\dot\beta C_\gamma+\dot\alpha S_\beta S_\gamma)+I_2C_\gamma\left[\dot\alpha\dot\beta C_\beta S_\gamma+\dot\gamma(\dot\alpha S_\beta C_\gamma-\dot\beta S_\gamma)\right]\end{aligned}$$

and $C_3=-I_3\dot\alpha\dot\beta S_\beta$.

$$\mathbf{Q_T}=\begin{bmatrix}F_x+mgS_\beta C_\gamma & F_y-mgS_\beta S_\gamma & F_z-mgC_\beta\end{bmatrix}^{\mathrm{T}} \tag{A.3}$$

and

$$\mathbf{Q_R}=\begin{bmatrix}Q_1 & Q_2 & Q_3\end{bmatrix}^{\mathrm{T}} \tag{A.4}$$

where $Q_1=-(T_x+G_1)S_\beta C_\gamma+(T_y+G_2)S_\beta S_\gamma+(T_z+G_3)C_\beta$,

$Q_2=(T_x+G_1)S_\gamma+(T_y+G_2)C_\gamma$

and $Q_3=(T_z+G_3)$

and where $G_1=mgy_cC_\beta-mgz_cS_\beta S_\gamma$, $G_2=-mgx_cC_\beta-mgz_cS_\beta C_\gamma$, and $G_3=mgy_cS_\beta C_\gamma-mgx_cS_\beta S_\gamma$.

APPENDIX B

PARAMETERS OF THE DMP MODEL

The unknowns (*k, n,* $\bar{\ell}$, and m_j where $j = 0, \ldots, k$) in the DMP model are solved by minimizing the error function (B.1) subject to

constraints imposed by the magnet geometry and a limited set of known field solutions:

$$E = \int_z \left[\Phi(z) - \Phi_A(z)\right]^2 dz \qquad \text{(B.1)}$$

where $\Phi_A(z)$ is the analytical solution along the magnetization axis. For a cylindrical PM, the potential and flux density along the z-axis can be expressed in closed form [14]:

$$\Phi_A(Z) = (M_o \ell / 4)\left[\left(A_- - |B_-|\right) - \left(A_+ - |B_+|\right)\right] \qquad \text{(B.2)}$$

$$B_A(Z) = \frac{1}{2}\mu_o M_o \left[\frac{|B_+|}{A_+} - \frac{|B_-|}{A_-} + c\right] \quad \text{where} \quad c = \begin{cases} 0 & \text{if } |Z| \geq 1 \\ 2 & \text{if } |Z| < 1 \end{cases} \qquad \text{(B.3)}$$

where $Z = z/(\ell/2)$; $\gamma = a/(\ell/2)$; $A_\pm = \sqrt{\gamma^2 + B_\pm^2}$ and $|B_\pm| = |Z \pm 1|$. For a given specified residual magnetic flux density, we have from (12):

$$\mathbf{B}(\ell/2) = \mathbf{B}_A(\ell/2) = -\mu_o \nabla \Phi_A\big|_{z=\ell/2} \qquad \text{(B.4)}$$

where **B** is given in (9). Since (10) accounts for the potential field along the magnetization axis, the remaining $(k \times n + 1)$ constraints are constructed from (8) and (9) along two other orthogonal directions. To avoid the singularity at $\mathbf{R} = \mathbf{R}'$, we choose

$$|R| = \lim_{\varepsilon \to 0}\left(|R'|_{\substack{\text{point} \\ \text{at surface}}} + \varepsilon_R\right)$$

where ε_R is a small positive number. For a cylindrical magnet, the field is uniform circumferentially and thus, we set the dipole moment $m_{ji} = m_j$. To minimize the field variation in the θ direction, we impose the following constraint on n:

$$\left.\frac{Max\left[\Phi(\theta)\right] - Mean\left[\Phi(\theta)\right]}{Mean\left[\Phi(\theta)\right]}\right|_{r=a, z=\ell/2} \times 100\% \leq \varepsilon_\theta \qquad \text{(B.5)}$$

where ε_θ is a specified (positive) error bound.

The procedure for modeling a PM is summarized as follows:

Step 1: Compute Φ_A and $\mathbf{B}_A$ analytically long the magnetization vector from (B.2) and (B.3) respectively

Step 2: Generate an initial set of spatial grid points (*k, n*).

Step 3: Formulate (7) and (8) in terms of the unknowns, $\bar{\ell}$ and m_{ji}.

Step 4: Find $\bar{\ell}$ and m_{ji} by minimizing (B.1) subject to a set of constraints constructed from (B.2) and (B.3). Error computed by (B.1) is saved.

Step 5: Check if the condition (B.5) is met. If no, increase *k* or *n*, and repeat from Step 3. If yes, the optimal parameters (*k*, *n*, $\bar{\ell}$ and m_{ji}) can be obtained by minimizing (B.1) using Step 4.